

RESPONSE OF DARK MATTER HALOS TO CONDENSATION OF BARYONS: COSMOLOGICAL SIMULATIONS AND IMPROVED ADIABATIC CONTRACTION MODEL

OLEG Y. GNEDIN¹, ANDREY V. KRAVTSOV², ANATOLY A. KLYPIN³, DAISUKE NAGAI²
 Submitted to the *Astrophysical Journal*

ABSTRACT

The cooling of gas in the centers of dark matter halos is expected to lead to a more concentrated dark matter distribution. The response of dark matter to the condensation of baryons is usually calculated using the model of adiabatic contraction, which assumes spherical symmetry and circular orbits. In contrast, halos in the hierarchical structure formation scenarios grow via multiple violent mergers and accretion along filaments, and particle orbits in the halos are highly eccentric. We study the effects of the cooling of gas in the inner regions of halos using high-resolution cosmological simulations which include gas dynamics, radiative cooling, and star formation. We find that the dissipation of gas indeed increases the density of dark matter and steepens its radial profile in the inner regions of halos compared to the case without cooling. For the first time, we test the adiabatic contraction model in cosmological simulations and find that the standard model systematically overpredicts the increase of dark matter density in the inner 5% of the virial radius. We show that the model can be improved by a simple modification of the assumed invariant from $M(r)r$ to $M(\bar{r})r$, where r and \bar{r} are the current and orbit-averaged particle positions. This modification approximately accounts for orbital eccentricities of particles and reproduces simulation profiles to within 10 – 20%. We present analytical fitting functions that accurately describe the transformation of the dark matter profile in the modified model and can be used for interpretation of observations.

Subject headings: cosmology: theory — dark matter : halos: structure — galaxies: formation — methods: numerical simulations

1. INTRODUCTION

During the past decade dissipationless cosmological simulations have shown that the density distribution within virialized halos of different masses can be described by an approximately universal profile (Dubinski & Carlberg 1991; Navarro et al. 1997; Moore et al. 1998). Although non-baryonic dark matter exceeds baryonic matter by a factor of $\Omega_{\text{dm}}/\Omega_{\text{b}} \approx 6$ on the average, the gravitational field in the central regions of galaxies is dominated by stars. In the hierarchical galaxy formation model the stars are formed in the condensations of cooling baryons in the halo center. As the baryons condense in the center, they pull the dark matter particles inward thereby increasing their density in the central region.

The response of dark matter to baryonic infall has traditionally been calculated using the model of adiabatic contraction. Eggen, Lynden-Bell, & Sandage (1962) were the first to use adiabatic invariants of particle orbits to estimate the effect of a changing potential in a contracting proto-galaxy. Zeldovich et al. (1980) used the adiabatic invariant approach to calculate the contraction of lepton halos in response to the cooling of baryons and set constraints on the annihilation cross-section of leptons. They also presented the first analytical expressions for adiabatic contraction (AC) for purely radial and circular orbits, as well as the numerical tests of such model. Barnes & White (1984) showed that the reaction of the particle orbits in spheroidal component to the slow growth of the disk in

their numerical experiments of disk and bulge evolution is indeed adiabatic and can be described by a simple model that assumes circular particle orbits and angular momentum conservation.

The present standard form of the AC model was introduced and tested numerically by Blumenthal et al. (1986, see also Ryden & Gunn 1987). This model assumes spherical symmetry, homologous contraction⁴, circular particle orbits, and conservation of the angular momentum: $M(r)r = \text{const}$, where $M(r)$ is the total mass enclosed within radius r . With these assumptions, the final dark matter distribution is calculated given the initial mass profiles $M_{\text{dm}}(r)$, $M_{\text{b}}(r)$ and final baryon profile $M_{\text{b}}(r_f)$:

$$[M_{\text{dm}}(r) + M_{\text{b}}(r)]r = [M_{\text{dm}}(r) + M_{\text{b}}(r_f)]r_f. \quad (1)$$

This model has been studied further by Ryden (1988, 1991) and Flores et al. (1993). It is routinely used in mass modeling of galaxies (e.g., Flores et al. 1993; Dalcanton et al. 1997; Mo et al. 1998; Courteau & Rix 1999; van den Bosch 2001; van den Bosch & Swaters 2001; Klypin et al. 2002; Seljak 2002) and clusters of galaxies (e.g., Treu & Koopmans 2002). The effect of the contraction of the dark matter distribution is important for studying star formation feedback on the centers of dark matter halos (Gnedin & Zhao 2002) and for comparing the abundance of dark matter halos and galaxies as a function of circular velocity (e.g., Gonzalez et al. 2000; Kochanek & White 2001). It is particularly important in calculations of the dark matter annihilation signal from the Galactic center (e.g., Gnedin & Primack 2004; Prada et al. 2004).

Despite recent advances in numerical simulations, the model of adiabatic contraction has never been tested in a cosmological context. The tests performed to date (Jesseit, Naab, & Burkert 2002) assume spherical symmetry

⁴ The halo can be imagined consisting of spherical shells which contract in radius but do not cross each other.

¹ Space Telescope Science Institute, 3700 San Martin Drive, Baltimore, MD 21218; ognedin@stsci.edu

² Dept. of Astronomy and Astrophysics, Kavli Institute for Cosmological Physics, The University of Chicago, Chicago, IL 60637; andrey.daisuke@oddjob.uchicago.edu

³ Astronomy Department, New Mexico State University, MSC 4500, P.O.Box 30001, Las Cruces, NM, 88003-8001; aklypin@nmsu.edu

and consider only the growth of a central concentration in an isolated halo. The hierarchical formation of halos is, in general, considerably more complex than the simple picture of quiescent cooling in a static spherical halo. Each halo is assembled via a series of mergers of smaller halos, with the cooling of gas and contraction of dark matter occurring separately in every progenitor. The gas can be re-heated by shocks during mergers and during accretion along the surrounding filaments. Also, some objects may undergo dissipationless mergers after the gas is exhausted or the cooling time becomes too long. It was argued that dissipationless evolution erases the effect of gas cooling on the DM distribution (Gao et al. 2004).

In this paper we consider the effect of dissipation on the dark matter distribution in high-resolution cosmological simulations. We also present the first test of the AC model in the self-consistent simulations of hierarchical structure formation and propose a simple modification which describes numerical results more accurately.

2. COSMOLOGICAL SIMULATIONS

We analyze high-resolution cosmological simulations of eight group and cluster-sized and one galaxy-sized systems in a flat Λ CDM model: $\Omega_m = 1 - \Omega_\Lambda = 0.3$, $\Omega_b = 0.043$, $h = 0.7$ and $\sigma_8 = 0.9$. The simulations are performed with the Adaptive Refinement Tree (ART) N -body+gasdynamics code (Kravtsov 1999; Kravtsov, Klypin, & Hoffman 2002), an Eulerian code that uses adaptive refinement in space and time and (non-adaptive) refinement in mass to achieve the high dynamic range needed to resolve the halo structure.

The cluster simulations have a peak resolution of $\approx 2.44h^{-1}$ kpc and DM particle mass of $2.7 \times 10^8 h^{-1} M_\odot$ with only a region of $\sim 10h^{-1}$ Mpc around each cluster adaptively refined. We analyze each cluster at a late epoch ($0 < z < 0.43$), when it appears most relaxed. This minimizes the noise introduced by substructure on the azimuthally-averaged mass profiles. The virial masses⁵ of the clusters range from $\approx 10^{13} h^{-1} M_\odot$ to $3 \times 10^{14} h^{-1} M_\odot$.

The galaxy formation simulation follows the early ($z \geq 4$) evolution of a galaxy that becomes a Milky Way-sized object at $z = 0$ in a periodic box of $6h^{-1}$ Mpc. The simulation is stopped at $z \approx 3.3$ due to limited computational resources. At $z = 4$, the galaxy already contains a large fraction of its final mass: $\approx 2 \times 10^{11} h^{-1} M_\odot$ within $30h^{-1}$ kpc. The DM particle mass is $9.18 \times 10^5 h^{-1} M_\odot$ and the peak resolution of the simulation is $183h^{-1}$ comoving pc. This simulation is presented in Kravtsov (2003), where more details can be found.

For each halo, we analyze two sets of simulations which start from the same initial conditions but include different physical processes. The first set of simulations follows the dynamics of gas “adiabatically”, i.e. without radiative cooling. The second set of simulations (hereafter CSF) includes star formation, metal enrichment and thermal supernovae feedback, metallicity- and density-dependent cooling, and heating due to the extragalactic UV background. Star formation in the cluster simulations is implemented using the standard Kennicutt’s law and is allowed

⁵ We define the virial radius, r_{vir} , as the radius enclosing an average density of 180 times the mean density of the Universe at the analyzed epoch.

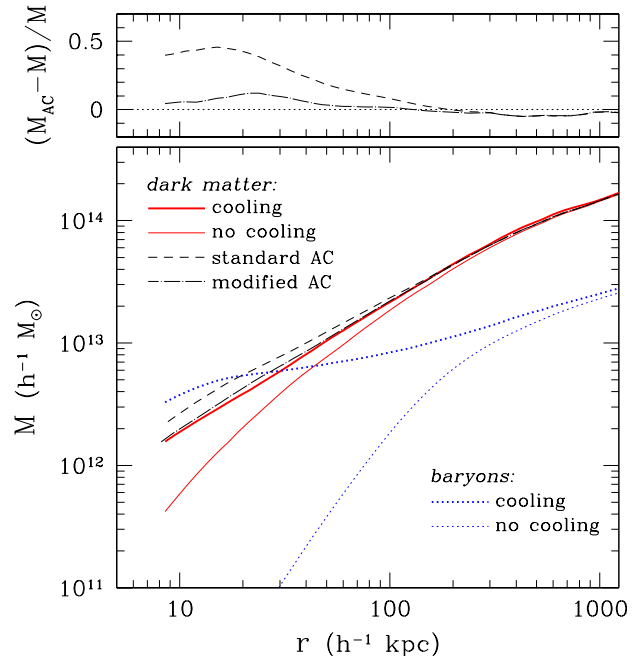


FIG. 1.— Mass profile of one of the clusters as a function of physical radius. The *solid* and *dotted* lines show the profiles of dark matter and baryons (stars+gas) in the adiabatic (*thin*) and cooling (*thick*) runs, respectively. The *dashed* curve shows the prediction of the standard adiabatic contraction model, while *dot-dashed* curve shows the improved model. The profiles are truncated at four resolution elements of the simulation. *Top panel*: relative mass difference between the adiabatic contraction model and the DM profile in the CSF simulation. The *dashed* line is prediction of the standard AC model, while *dot-dashed* line shows our modified model.

to proceed in regions with temperature $T < 10^4$ K and gas density $n > 0.1 \text{ cm}^{-3}$. In the galaxy formation run, the star formation rate is proportional to the gas density and stars are allowed to form at densities $n > 50 \text{ cm}^{-3}$. The difference in star formation prescriptions in galaxy and cluster simulations, accounts for the difference in spatial resolution. The prescription used in the galaxy formation run is more appropriate when applied at the scale of tens of parsecs (see Kravtsov 2003, for discussion).

To identify dark matter halos we use a variant of the Bound Density Maxima algorithm (Klypin et al. 1999). Dark matter particles in the high-resolution region of the simulation are assigned a local density calculated by using 24-particle SPH kernel. We identify local density peaks on a scale of $100h^{-1}$ kpc and analyze the density distribution and velocities of the surrounding particles to test whether a given peak corresponds to a gravitationally bound object. In this study we only consider host halos: those that do not lie within a larger virialized halo. We identify the center of each halo with the position of the DM particle with the highest local density. Based on the convergence studies for the ART code (Klypin et al. 2001; Tsitsiomi et al. 2004), we truncate the dark matter profiles at $4\Delta x_{\text{min}}$, where Δx_{min} is the smallest cell size: $2.44h^{-1}$ and $0.183h^{-1}$ comoving kpc in the cluster and galaxy formation runs, respectively.

3. EFFECTS OF COOLING ON MATTER DISTRIBUTION

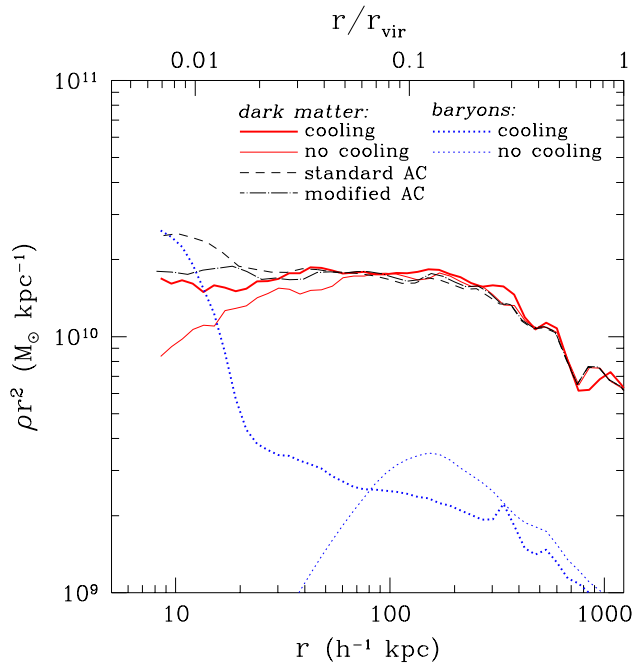


FIG. 2.— Density profile of the cluster shown in Figure 1, with the same line types. In order to emphasize the differences at small radii, we plot the combination $\rho(r)r^2$ which is roughly constant for isothermal distributions. Physical radius is shown in $h^{-1} \text{ kpc}$ (bottom axis) and as a fraction of the virial radius, r_{vir} (top axis).

We start by comparing the spherically averaged distribution of baryons and dark matter in the adiabatic and CSF simulations. The comparison reveals the effect of cooling and star formation because the two simulations for each object have the same initial conditions. Note that the cluster simulations likely suffer from the “overcooling” problem: the fraction of gas in the cold phase is about a factor of $\sim 2 - 3$ higher than suggested by observations (e.g., Balogh et al. 2001). The effect of cooling on mass distribution is thus likely overestimated. For the purposes of the present study, however, this is acceptable. In fact, the larger effect of cooling allows us to emphasize the difference between the simulations and the model.

The mass and density profiles of a representative cluster are shown in Figures 1 and 2. These figures show that cooling leads to an increase in the dark matter density within $r \lesssim 50 h^{-1} \text{ kpc}$ or $r/r_{\text{vir}} \lesssim 0.04$ (see also Tissera & Dominguez-Tenreiro 1998). The mass profile is affected substantially at $r < 0.1 r_{\text{vir}}$ and the change increases with decreasing radius. At larger radii the average mass profile is not sensitive to baryon dissipation and the differences between the adiabatic and CSF runs are the result of the slightly different location of massive substructures.

Figure 3 shows the density profiles in the galaxy formation run at $z = 4$. Qualitatively, the effect of cooling is similar to that seen in the cluster simulations. In this case, however, DM density in the CSF run is enhanced within a larger radius, $r/r_{\text{vir}} \lesssim 0.1$. Also, baryons dominate the total density at $r/r_{\text{vir}} \lesssim 0.03$ in the galaxy simulation, while in the cluster simulation they dominate only at $r/r_{\text{vir}} \lesssim 0.01$. The difference is due to the considerably higher fraction of cold ($T < 10^4 \text{ K}$) gas in the galaxy run: 80% at $z = 4$ versus $\sim 0.2 - 0.3$ in the cluster sim-

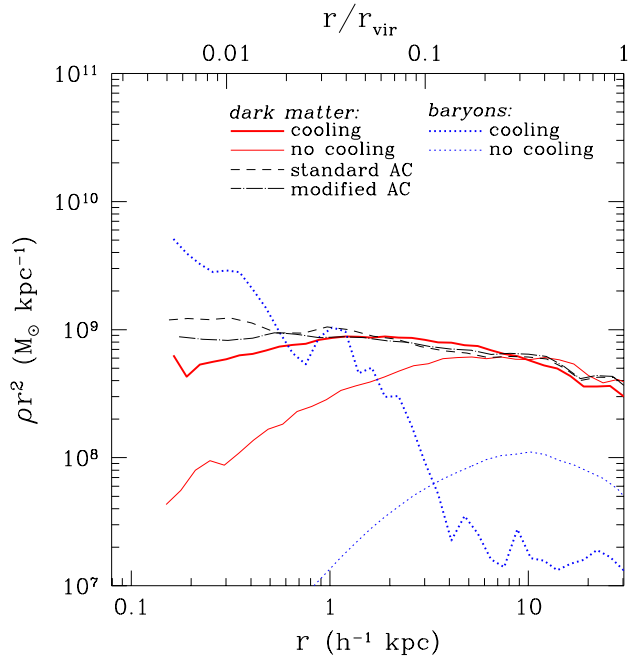


FIG. 3.— Density profile in the galaxy formation run at $z = 4$ as a function of physical radius. Lines types are as in Figure 1.

ulations. These fractions reflect a difference in densities, temperatures, and cooling times of the gas in clusters and high-redshift galaxies. Note that there are differences in the mix of gas and stars. At $z \lesssim 0.5$, most of the baryon mass within the central regions of clusters is in the stellar component of the cD galaxy. In the galaxy run, on the other hand, more than 80% percent of baryons in the dense central disk are still in the gaseous form. The cluster and galaxy formation simulations thus probe qualitatively different regimes of the evolution of central baryon condensation.

4. TESTING THE ADIABATIC CONTRACTION MODEL

4.1. Standard Model

In this section we test the standard prescription for adiabatic contraction, given by equation (1). In order to calculate the model prediction for the final dark matter distribution in the CSF run, we use the mass profile of baryons $M_b(r_f)$ from this run and the mass profiles of dark matter and baryons from the adiabatic simulation at the same epoch. We consider adiabatic profiles as the initial profiles for the model, $M_{\text{dm}}(r)$ and $M_b(r)$. We then use equation (1) to predict the DM distribution in the CSF run and compare the model prediction to the actual dark matter profile in simulation.

The prediction of the standard AC model is shown in Figures 1, 2, and 3 by the dashed lines. The fractional deviations of the model prediction from the simulation for all analyzed systems are shown in Figure 4. The standard model predicts the overall mass enhancement but systematically overestimates its magnitude in the inner regions, at $r/r_{\text{vir}} \lesssim 0.1$. This effect has already been noticed in the original study by Blumenthal et al. (1986). Possible causes of the discrepancy could be (1) non-spherical mass distribution and substructure; (2) simultaneous evolution

of the dark matter and baryonic components; and (3) the assumption of circular orbits. In the next section we investigate whether the model can be improved by accounting for orbital eccentricities.

4.2. Modified model

The orbits of particles in dark matter halos in simulations are highly eccentric (e.g., Ghigna et al. 1998). The combination $M(r)r$ for such orbits varies with the orbital phase and is not an adiabatic invariant. The conserved quantities for eccentric orbits are the angular momentum, J , and the radial action,

$$I_r \equiv \frac{1}{\pi} \int_{r_p}^{r_a} v_r dr, \quad (2)$$

where v_r is the radial velocity, and r_p and r_a are the peri- and apo-center, respectively. For non-crossing spherical shells, the radial velocity can be expressed using the first integrals of motion C (e.g., Ryden & Gunn 1987; Gnedin & Ostriker 1999) as

$$v_r = \left(\frac{2GM(r)}{r} - \frac{J^2}{r^2} + C \right)^{1/2}. \quad (3)$$

The parameters C change when shells cross, although the sum over all shells is constant. In the case of purely radial orbits in a self-similar potential, we have $J = 0$ and $r_p = 0$, so that $I_r^2 \propto M(r_a)r_a$, and therefore the combination $M(r_a)r_a$ is conserved during a slow change of the potential (Blumenthal et al. 1986). The potentials of dark matter halos are, in general, not self-similar while the angular momentum is not zero, and the invariants cannot be reduced to a simple combination of r and $M(r)$ that would be useful for predicting the final dark matter profile.

It is interesting to check, though, if a combination that depends on the average radius along the orbit, \bar{r} , rather than the instantaneous value r or the maximum r_a , is conserved better than $M(r)r$ or $M(r_a)r_a$. The orbit-averaged radius is

$$\bar{r} = \frac{2}{T_r} \int_{r_p}^{r_a} r \frac{dr}{v_r}, \quad (4)$$

where T_r is the radial period.

As a first check, we consider isochrone potential, $\Phi_{\text{iso}} \propto -[1 + (1 + (r/r_s)^2)^{1/2}]^{-1}$ (Binney & Tremaine 1987), for which the radial action is known analytically as a function of E and J . We choose the angular momentum that corresponds to realistic eccentricities ($e \approx 0.7$): $J = J_c(E)/\sqrt{3}$, where $J_c(E)$ is the angular momentum of a circular orbit of energy E . We then check whether the combination $M(\bar{r})\bar{r}$ is proportional to I_r^2 for all orbits. The ratio $M(\bar{r})\bar{r}/I_r^2$ is constant at small radii ($r \ll r_s$) and large radii ($r \gg r_s$) but varies in between by 50%. An alternative, the apocenter ratio $M(r_a)r_a/I_r^2$ exhibits considerably larger variation between the asymptotes, by about 300%. Thus the combination $M(\bar{r})\bar{r}$ is a better proxy to the invariant than $M(r_a)r_a$.

In order to study more realistic orbits with the energies and angular momenta relevant for cosmological simulations, we use a separate set of high-resolution collisionless simulations of three Milky Way-sized halos and one Virgo cluster-sized halo. Galaxy-sized halos have about one million DM particles within their virial radius (see

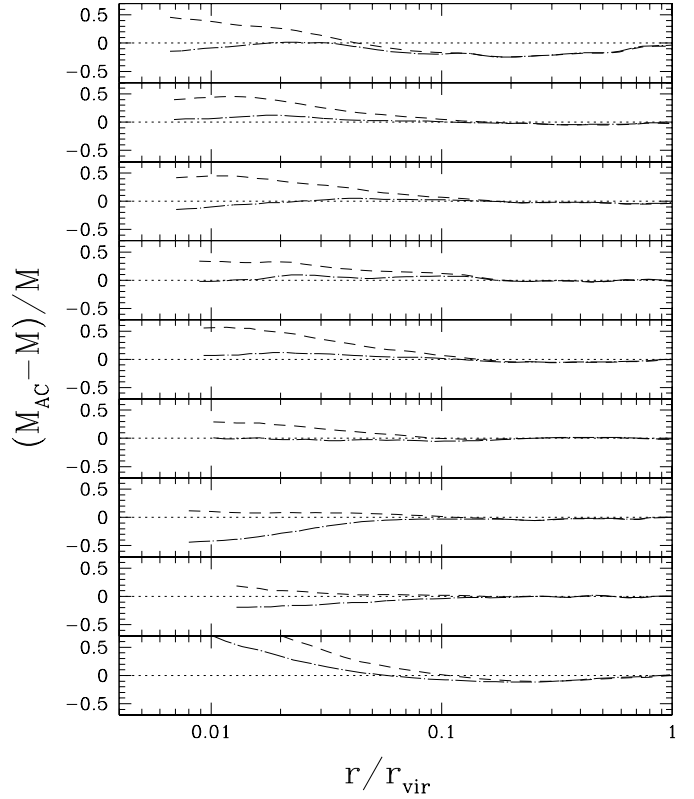


FIG. 4.— Fractional differences of the mass profiles predicted by the adiabatic contraction models and the simulation profiles for eight clusters (top eight panels) and one galaxy formation run (the bottom panel). Dashed lines correspond to the standard model and dot-dashed lines show our modified model, eq. (6). The cluster in the top panel is experiencing a merger event with a comparable mass cluster, which can be seen as an excursion of the profile at $r \sim 0.2r_{\text{vir}}$.

Kravtsov et al. 2004, for details), while the cluster-sized halo has approximately eight million particles (Tasitsiomi et al. 2004). All runs have spatial resolution $\lesssim 10^{-3} r_{\text{vir}}$. We approximate the potential of each halo with a spherically symmetric NFW profile (Navarro et al. 1997) parameterized by the mass and maximum circular velocity measured in the simulations. We then integrate the orbits in this potential starting with the particle positions and velocities given by the simulations and calculate the radial action (eq. 2) numerically.

The orbits have a distribution of eccentricities that is very similar to the isotropic distribution in analytical potentials studied by van den Bosch et al. (1999): the 20%, 50%, and 80% quartiles are $e = 0.39, 0.61, 0.79$, respectively. Given such a wide eccentricity distribution, the orbit-averaged radius \bar{r} varies for particles at a given current radius r depending on the orbital phase. Nevertheless, the mean relation at $10^{-3} \lesssim r/r_{\text{vir}} \lesssim 1$ can be described by a power law function

$$\bar{x} = Ax^w, \quad x \equiv r/r_{\text{vir}}, \quad (5)$$

with small variations in the parameters A and w from halo to halo and from epoch to epoch. The mean values are $A \approx 0.85 \pm 0.05$ and $w \approx 0.8 \pm 0.02$, which we use as our fiducial parameters. This power-law dependence reflects

typical energy and eccentricity distributions of particles in cold dark matter halos. At $x < 0.44$ the average radius is larger than the current radius, while at $x > 0.44$ it is smaller.

The distribution of eccentricities at a current radius r leads also to a distribution of each combination $M(r)r$, $M(r_a)r_a$, and $M(\bar{r})\bar{r}$. None of these combinations is proportional to the invariant I_r^2 for individual orbits. What we are looking for is a proxy to the invariant for an ensemble of orbits representing a spherical shell. Such a proxy would allow us to calculate the transformation of the dark matter profile imagined of consisting of spherical shells. Therefore, instead of individual particle orbits we look at the average ratios $M(r_a)r_a/I_r^2$ and $M(\bar{r})\bar{r}/I_r^2$ in radial bins. Across all bins the average ratio $M(r_a)r_a/I_r^2$ varies by a factor 3.4, while the ratio $M(\bar{r})\bar{r}/I_r^2$ varies only by a factor 2.2. Therefore, our insight gained from analytic orbits in isochrone potential is still valid for isotropic orbits in NFW potential: the combination $M(\bar{r})\bar{r}$ is a better proxy to the invariant. Moreover, we have found that the mixed combination $M(\bar{r})r/I_r^2$ varies even somewhat less, by a factor of 2 across all radii. This latter combination thus is our best proxy for the radial action.

Motivated by these considerations, we propose a modified adiabatic contraction model based on conservation of the product of the current radius and the mass enclosed within the orbit-averaged radius:

$$M(\bar{r})r = \text{const.} \quad (6)$$

Using equation (5) we compare our gasdynamic simulations with this modified model.

Figures 1–4 show that the modified model provides a more accurate description of the simulation results than the standard model for most of the objects. Although there are still deviations of the model and simulation profiles, there is no systematic over- or under-prediction of the mass for all objects. Typical deviations are $\lesssim 10\%$. Note that for the high-redshift galaxy disk both the standard and modified AC models overpredict the mass profile significantly, although the modified model is still closer to the simulated profile. The discrepancy is large in the inner kiloparsec where the most of the mass is in the thin gaseous disk. The adiabatic contraction model cannot be applied in such regime and further numerical simulations are needed to investigate the dark matter distribution in the galactic center.

An interesting question is why the adiabatic contraction works as well as it does? Although the model assumes that gas cooling affects DM distribution in the final object adiabatically, the particles experience contraction in separate unconnected halos and undergo some degree of violent relaxation in subsequent mergers. To check the evolution of individual particle orbits we have compared their physical distance r to the center of the main progenitor and quantities $M(r)r$, $M(\bar{r})r$ at a number of epochs from $z = 0$ to $z = 4$ for one of the clusters. There is a substantial scatter in the relation of these quantities between the present and higher redshifts. However, some interesting trends for the averages of $M(r)r$ and $M(\bar{r})r$ can be observed. First of all, we find that both radii and products of radii and mass evolve as the object grows hierarchically, especially during major mergers. However, between mergers, during the periods when a substantial

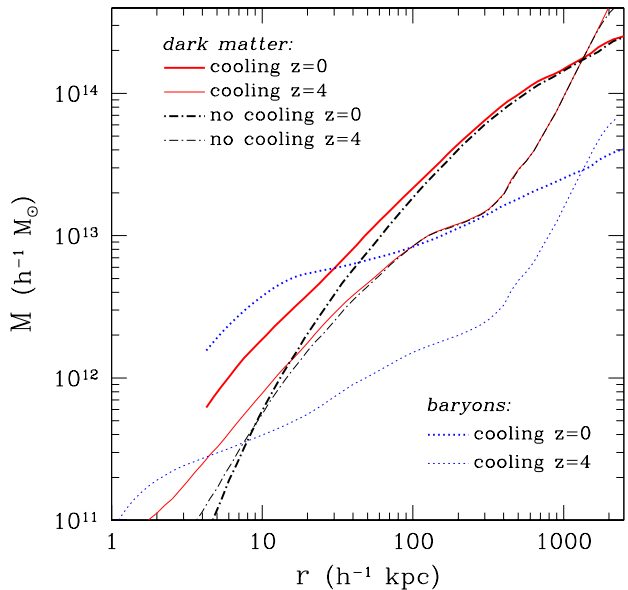


FIG. 5.— The effect of gas cooling on the mass profile at different epochs for the cluster shown in Figures 1 and 2. *Thin* and *thick* lines show the profiles at $z = 4$ and $z = 0.18$, respectively: *dotted* lines — profiles for baryons (gas+stars) in the CSF run; *dot-dashed* lines — profiles of DM in the adiabatic run; *solid* lines — DM profiles in the CSF run.

amount of gas cools, $M(r)r$ and $M(\bar{r})r$ seem to be conserved. The latter combination is conserved better than the former, which may explain why our modification to the AC model is successful.

We find also that most ($\approx 70\%$) particles within the central $25h^{-1}$ kpc of the cluster center at $z = 0$ come from a single progenitor at $z = 1$. This progenitor is not the most massive but has the highest central density. When it merges with a more massive progenitor at $z \approx 0.5$ to form the final system, its particles are most tightly bound and end up dominating the mass in the central region of the merger remnant. This is consistent with other merger simulations which show that particles from the progenitor with the densest central region dominate the inner regions of the remnant (Boylan-Kolchin & Ma 2004).

5. HOW STEEP IS THE CENTRAL DARK MATTER PROFILE?

Dark matter distribution in the central regions of galaxies and clusters is important for testing the CDM paradigm and interpreting the observations. It is generally believed that dissipation by baryons would steepen the dark matter profile (Barnes & White 1984; Blumenthal et al. 1986; Ryden & Gunn 1987). However, Loeb & Peebles (2003) and Gao et al. (2004, hereafter G04) recently suggested that after an early epoch of cooling and rapid star formation, subsequent dissipationless mergers would erase the cooling-induced central concentration of dark matter. They put forth a hypothesis that the NFW profile is a dynamical attractor, in the sense that remnants of dissipationless mergers are driven to the central profile with the cusp $\rho(r) \propto r^{-1}$, even if their progenitors have steeper DM profiles. As a supporting argument G04 use obser-

vation that the density in the inner regions of halos in *dissipationless* simulations is approximately constant after the initial period of rapid mass growth. The attractor hypothesis together with observation that stars dominate gravitationally in the centers of galaxies leads to the conclusion that the dark matter profile in galaxies which experienced dissipationless mergers should be shallower than r^{-1} .

The results of our simulations do not support this conclusion. Given the importance of the problem, it is worth discussing the differences between the simulations and analysis of G04. Figure 5 compares the mass profile of the cluster shown in Fig. 1 at $z = 0$ with its most massive progenitor at $z = 4$. We first verify that in adiabatic simulations the DM mass profile in the inner $\approx 10h^{-1}$ kpc is approximately constant from $z = 4$ to the present epoch, in agreement with analyses of Fukushige & Makino (2001) and G04. Within the physical radius $r = 10h^{-1}$ kpc the enclosed mass is $M(r) \approx 5 \times 10^{11} h^{-1} M_{\odot}$ at both epochs.

The evolution is very different in the run with cooling and star formation. By $z = 4$, a considerable stellar mass ($\sim 3 \times 10^{11} h^{-1} M_{\odot}$) has formed within $10h^{-1}$ kpc of the center of the main cluster progenitor. However, the baryon mass within central $10h^{-1}$ kpc continues to grow and increases by a factor of ten between $z = 4$ and $z = 0.2$. Approximately 50% and 70% of those stars form at $z < 1$ and $z < 2$, respectively. Note that the stars and cold gas in cluster cores are accumulated both due to direct cooling in the core and via accretion during mergers (Motl et al. 2004).

As can be seen in Figure 5, such substantial increase in the baryon mass leads to the increase of the DM density in the inner regions. The final dark matter mass within $10h^{-1}$ kpc is $\approx 2 \times 10^{12} h^{-1} M_{\odot}$, or a factor of four larger than the mass in the adiabatic simulation. Therefore, one of the major differences between our simulations and analysis of G04 is that in the simulation the density of both baryons and dark matter increases at lower redshifts, while G04 assume that the density of DM decreases as the total mass distribution is driven to the NFW profile. Note also that G04 assume that star formation and cooling in the centers of massive ellipticals effectively stops at $z \sim 2 - 3$, while in our simulations cooling and star formation continue at lower redshifts with more than half of the stars formed at $z < 2$. This can be a deficiency of simulations which, as we mentioned above, suffer from the overcooling problem. The fraction of baryons in the cold gas and stars within the virial radius of clusters at $z = 0$ in our simulations is in the range $\sim 0.3 - 0.4$, at least a factor of two higher than observed for the systems of the mass range we consider (Lin, Mohr, & Stanford 2003). The overcooling and relatively late star formation is a generic problem of cosmological simulations and is hardly realistic. It likely indicates that some mechanism suppressing cooling is needed.

If we follow G04 and assume that cooling ceases at late epochs, the question is then whether subsequent dissipationless evolution erases the prior effect of cooling on the concentration of DM and drives the overall stellar+DM profile to the NFW form, as required by the attractor hypothesis. Several recent studies have considered the effect of major mergers and dynamical effects of substructure

on the dark matter profiles in the inner regions of halos (Dekel et al. 2003a,b; El-Zant et al. 2003; Boylan-Kolchin & Ma 2004; Ma & Boylan-Kolchin 2004; Nipoti et al. 2004). Dissipation of the orbital energy of massive subhalos by dynamical friction can heat the dark matter particles of the host and reduce the DM density in the inner regions. On the other hand, DM particles of the sinking subhalos replace the host particles and the overall central density profile stays approximately constant or even becomes steeper, depending on internal structure, spatial distribution, and orbital parameters of subhalos (Ma & Boylan-Kolchin 2004).

Major mergers can lead to a more drastic and violent rearrangement of matter in halos compared to the effects of substructure. Boylan-Kolchin & Ma (2004) present a set of merger simulations, which are most relevant for our discussion. They show that mergers of halos with constant density cores produce a remnant with a constant density core, but mergers of the cored and cuspy halos produce a cuspy remnant. Their analysis shows that the initial cusp is remarkably stable and the density distribution of the merger remnants retains memory of the density profiles of their progenitors. This is in good agreement with the analysis of merger experiments presented by Kazantzidis et al. (2004). The merger remnant of the DM halos with a steep inner density profile ($\rho(r) \propto r^{-1.8}$) retains the initial slope of the inner cusp. The mergers of halos with embedded stellar disks also produce DM halos with the inner cusp not shallower than the initial.

The attractor hypothesis is thus not supported by dissipationless simulations. The effects of dissipation on the DM distribution in the progenitors is retained, at least to a certain extent, in the density distribution of their descendant. The overall effect of merging is just to mix dark matter particles within the same distribution, while baryon dissipation leads to a significant increase of the dark matter density.

Finally we note that for the halos that harbor a supermassive black hole the density distribution within its sphere of influence (typically 10 – 100 pc) is determined by the interaction between the black hole, stars, and DM (e.g., Gnedin & Primack 2004).

6. DISCUSSION AND CONCLUSIONS

We have analyzed results of self-consistent cosmological simulations of eight galaxy clusters and one galactic halo with and without cooling and star formation. The comparison of adiabatic and CSF simulations shows that cooling increases the total density and the density of dark matter at $r \lesssim 0.1r_{\text{vir}}$. This agrees qualitatively with results of other recent simulations (Tissera & Dominguez-Tenreiro 1998; Lewis et al. 2000; Pearce et al. 2000; Valdarnini 2002). Note that at $r \gtrsim 0.01r_{\text{vir}}$ modern dissipationless simulations have reached a robust convergence (e.g., Diemand et al. 2004). We conclude therefore that further progress in making predictions for the DM distribution on small scales requires studying gas dissipation. The effect of cooling also needs to be taken into account when comparing the simulations with observations.

We have presented the first tests of the adiabatic contraction model in self-consistent high-resolution cosmolog-

ical simulations.⁶ We find that the standard AC model systematically overpredicts the increase of the dark matter density in the inner $\lesssim 0.05r_{\text{vir}}$. We have shown that the model can be improved by a simple modification of the assumed conserved invariant from $M(r)r$ to $M(\bar{r})r$, where r and \bar{r} are the current and orbit-averaged particle positions. This modification approximately accounts for the eccentricity of particle orbits. Our improved model describes profiles in simulations considerably better than the standard model, with the average accuracy of 10–20%.

Jesseit et al. (2002) have used controlled simulations of isolated spherical halos with a growing central concentration of baryons to test the validity of the standard AC model. They find that generally the standard model describes their simulation more accurately than we find in our tests against cosmological simulations. The density distributions of their model halos are realistic and it is not immediately clear what is the cause of the difference. Possible reasons are differences in (i) orbital distributions for the isolated halos versus cosmological halos formed by mergers; and (ii) formation histories and degree of violent relaxation. In particular, Jesseit et al. (2002) find that the standard model significantly overpredicts the contraction effect when the growth of the central baryon concentration is rapid compared to the dynamical time of the halo.

Given that dark matter halos assemble via mergers and violent relaxation, it is somewhat of a puzzle that the adiabatic contraction model reproduces the results of simulations so well. The success of the model seems to imply that the effect of the central baryon condensation on the dark matter distribution is independent of the way in which this condensation is assembled. At the same time, it may simply be due to the fact that the central region is dominated by particles from a single densest progenitor. If the progenitor halo contracts in response to the cooling of baryons early on and then approximately preserves the shape of its inner density profile during subsequent mergers, as suggested by merger simulations (see § 5), the AC model applied to the final mass distribution is expected to work.

In Appendix we provide analytical fitting functions that describe the contraction of an initial NFW profile in our modified model. These functions can aid in interpretation of observations of galaxy halos and clusters of galaxies. We show that the inner slope of the dark matter density profile γ is determined by the shape of the baryon profile (see eq. [A12]). For the specific cases of the exponential disk and Hernquist model, both the baryon and the contracted DM profiles have the asymptotic slope $\gamma = 1$.

Our results have several implications for the efforts to test predictions of the CDM model observationally. The test that received much attention in the last decade is the density distribution in the inner regions of galaxies and clusters. Extensive convergence studies have shown that modern highest-resolution dissipationless simulations agree in their predictions: the average logarithmic slope of

the density profile at $r = 0.01r_{\text{vir}}$ is $\gamma \approx 1.3$ with a substantial scatter of ± 0.3 from object to object (Fukushige et al. 2004; Tasitsiomi et al. 2004; Navarro et al. 2004; Reed et al. 2004; Diemand et al. 2004). At the same time, despite a significant decrease in the smallest reliably resolved scale, the logarithmic slope continues to get shallower with decreasing radius without reaching an asymptotic value. For the purposes of the present discussion, it suffices that dissipationless simulations have converged at the scales where the effects of dissipation become important.

Observational measurements of the dark matter density distribution are notoriously difficult. Several approaches have been used but in each case opposite conclusions are reached by different researchers, often after analyzing the same data. The rotation curves of dark matter dominated dwarf and low-surface brightness galaxies tend to favor density profiles shallower than predicted by CDM (e.g., Simon et al. 2003; de Blok et al. 2003). The results, however, are sensitive to the resolution of rotation curves, presence of bulges and non-circular motions, and for many galaxies the profiles can be reconciled with theoretical expectations (e.g., Swaters et al. 2003; Rhee et al. 2004). The analysis of density distribution for bright galaxies is complicated by the uncertain contribution of stars to the total mass profile (e.g., Treu & Koopmans 2002; Mamon & Lokas 2004). Some analyses tend to favor inner slopes shallower than predicted by CDM (e.g., Gentile et al. 2004), but others deduce slopes of the inner profiles (at least marginally) consistent with predictions (Treu & Koopmans 2002, 2004; Koopmans & Treu 2003; Jimenez et al. 2003).

The density distribution in galaxy clusters can, in principle, provide a cleaner test of the models because effects of “gastrophysics” on the DM distribution are expected to be smaller and simpler. The advances in lensing analyses, X-ray observations, and high-resolution spectroscopy allow observers to obtain constraints on the DM distribution using a variety of techniques. Recent observational analyses using strong lensing (e.g., Tyson et al. 1998), high-resolution X-ray imaging (Ettori et al. 2002; Katayama & Hayashida 2004, but see David et al. 2001 and Arabadjis et al. 2002), and lensing+velocity dispersion measurements for the central galaxy (Sand et al. 2002, 2004) seem to favor shallow ($\gamma \lesssim 0.5 - 1$) inner density distributions. If these observational results stand, it would be a major problem for the CDM because dissipation generally makes the discrepancy worse.

Many of the systematic effects and validity of the key assumptions in such measurements are yet to be explored. For example, deviations from spherical symmetry in the mass distribution allows for the inner slopes of $\gamma \gtrsim 1$ (Dalal & Keeton 2004; Bartelmann & Meneghetti 2004). Some of our results also call into question the assumptions used to derive observational constraints. For example, it is often assumed that at small scales the DM profile can be well approximated by a power law, $\rho(r) \propto r^{-\gamma}$. It is also assumed that dissipation would steepen the profile predicted from dissipationless simulations while retaining its power law form. As we show in Appendix, however, the steepening of the profile due to cooling is in general scale-dependent. For realistic cases, the profiles of dark matter and baryons at $r \lesssim 0.01r_{\text{vir}}$ should be quite similar. These scales are exactly where the profiles of massive ellipticals

⁶ After this paper was completed we have learned of a different study of the AC model in cosmological simulations (Gottbrath & Steinmetz, 2000 unpublished). These authors found that the AC model works adequately at the resolved scales. However, the resolution of the simulations used in their study is considerably lower than resolution of our simulations, and the scales where we find significant discrepancy between AC model and simulations were not resolved.

and central cluster galaxies are probed by spectroscopic measurements in observations. If incorrect assumptions are made about the DM distribution, there is a danger of oversubtracting the contribution of baryons to the total profile. Stars dominate the inner region and only a small overestimate of the stellar mass-to-light ratio could lead to a much lower residual density of dark matter.

The fact that the standard AC model overpredicts the effect of cooling on mass distribution means that observational analyses that use the standard model (e.g., Treu & Koopmans 2002, 2004) provide somewhat less stringent limits on γ than claimed. Our results for the disk galaxy at high redshift show that even the improved model can still overestimate the effect in the inner region of the gaseous disk. Extrapolation of the model to very small radii, as is often done in predictions of the dark matter annihilation signal, can therefore be dangerous. Further high-resolution gasdynamics simulations are needed to probe the effect of cooling in the centers of dark matter halos.

We would like to thank Joel Primack and Simon White for discussions and useful comments on the manuscript, and Andrew Zentner and Stelios Kazantzidis for discussions and analysis of the density profiles in the controlled merger experiments. We would also like to acknowledge Bocage of San Saba Vineyards. This work was supported by the National Science Foundation under grants AST-0206216 and AST-0239759 to the University of Chicago, by NASA through grant NAG5-13274, and in part by grant by the Kavli Institute for Cosmological Physics (KICP), an NSF Physics Frontier Center, through grant NSF PHY-0114422. O.Y.G. is supported by the STScI Fellowship. D.N. is supported by the NASA Graduate Student Researchers Program and by NASA LTSA grant NAG5-7986. The simulations presented here were performed on the IBM SP4 system (**copper**) of the National Computational Science Alliance.

APPENDIX

ANALYTICAL FITS FOR THE CONTRACTED DARK MATTER MASS PROFILE

In many applications it can be useful to have an analytical formulae to estimate the compression of dark matter due to baryonic condensation. We find that a simple procedure described below provides an accurate fit for the compression of an initial NFW profile.

We assume that the initial distributions of dark matter and baryons are both given by the NFW profile, $M_i(r)$, with a concentration parameter c . Subsequently the baryons cool and form stars and their final profile is given by $M_b(r_f)$, with the ratio of the baryon-to-total mass at the virial radius $M_b(r_{\text{vir}})/M_{\text{vir}} = f_b$. This ratio does not need to equal the universal baryon fraction and may deviate from it depending on the details of hierarchical formation and heating by the extragalactic UV flux. We consider two representative examples of the final baryon distribution: an exponential disk, which is appropriate for spiral galaxies, and a Hernquist model, which adequately describes the stellar profiles in elliptical galaxies. Both of these profiles are characterized by a scalelength r_b .

With the usual assumption of spherical homologous contraction, our goal is to calculate the final radius r_f of the dark matter particles initially located at $r > r_f$. It is useful to define the contraction factor $y \equiv r_f/r$. The equation we need to solve for y is

$$rM_i(\bar{r}) = [(1 - f_b)M_i(\bar{r}) + M_b(\bar{r}_f)]r_f. \quad (\text{A1})$$

Let us divide both sides of the equation by $M_i(\bar{r})r_f$ and use dimensionless radius $x \equiv r/r_{\text{vir}}$ and mass $m \equiv M/M_{\text{vir}}$:

$$\frac{1}{y} = 1 - f_b + \frac{m_b(\bar{x}y)}{m_i(\bar{x})}. \quad (\text{A2})$$

By definition, there is no contraction at the virial radius: $y(1) = 1$.

An important simplifying feature of the profiles we consider here (NFW, exponential disk, Hernquist model) is that at $x \ll 1$ the enclosed mass of all three profiles grows with radius as $m(x) \propto x^2$. The first two terms of the Taylor expansion at $x \ll 1$ are:

$$\begin{aligned} m_i(x) &= g_c \left[\log(1 + cx) - \frac{cx}{1 + cx} \right] \approx x^2 \frac{g_c c^2}{2} \left(1 - \frac{4c}{3}x + \dots \right) \\ m_b^H(x) &= f_b x^2 \left(\frac{1 + r_b}{x + r_b} \right)^2 \approx x^2 \frac{f_b(1 + r_b)^2}{r_b^2} \left(1 - \frac{2}{r_b}x + \dots \right) \\ m_b^E(x) &= f_b \left[1 - \left(1 + \frac{x}{r_b} \right) e^{-x/r_b} \right] \approx x^2 \frac{f_b}{2r_b^2} \left(1 - \frac{2}{3r_b}x + \dots \right), \end{aligned} \quad (\text{A3})$$

where $g_c \equiv [\log(1 + c) - c/(1 + c)]^{-1}$. Since our fit for the orbit-averaged radius \bar{x} is also a power-law ($\bar{x} = Ax^w$, $w = 0.8$) the mass ratio in eq. (A2) is constant at $x \ll r_b$, c^{-1} , and therefore $y(x)$ is approximately constant.

The finite value $y_0 \equiv y(0)$ is pivotal to constructing the fitting function for $y(x)$. We obtain the following equation for y_0 by retaining only the first terms of the Taylor expansion:

$$\frac{1}{y_0} = 1 - f_b + a y_0^{2w}, \quad (\text{A4})$$

where $a = 2f_b(1 + r_b)^2/(r_b^2 g_c c^2)$ for the Hernquist model and $a = f_b/(r_b^2 g_c c^2)$ for the exponential disk. There is no analytical solution for this algebraic equation, but we can obtain a very accurate approximate solution as follows. We first consider the standard model $w = 1$, for which eq. (A4) becomes a cubic equation. The solution is

$$y_{(1)} = \left(Q^{1/2} + \frac{1}{2a} \right)^{1/3} - \left(Q^{1/2} - \frac{1}{2a} \right)^{1/3}, \quad Q \equiv \left(\frac{1 - f_b}{3a} \right)^3 + \frac{1}{(2a)^2}. \quad (\text{A5})$$

There is only one real solution because Q is always positive. We then note that eq. (A4) with $w = 0.8$ differs from the cubic equation only at $a \gtrsim 1$. We can therefore obtain a solution for y_0 by matching the solution of the cubic equation for small a with the correct asymptote for large a . We find that the following modification produces the right asymptotic solution for $a > 1$:

$$y_{(w)} = \left(\hat{Q}^{1/2} + \frac{1}{2a} \right)^{1/(1+2w)} - \left(\hat{Q}^{1/2} - \frac{1}{2a} \right)^{1/(1+2w)}, \quad \hat{Q} \equiv \frac{1}{a^3} \left(\frac{1 - f_b}{1 + 2w} \right)^{1+2w} + \frac{1}{(2a)^2}. \quad (\text{A6})$$

Finally, we link the two asymptotes with a weight function that we empirically found to minimize the error of the fit:

$$y_0 = y_{(1)} e^{-2a} + y_{(w)} (1 - e^{-2a}). \quad (\text{A7})$$

The relative error of this fit, compared with the direct numerical solution, is only 0.2% on the average for all a and f_b . The asymptotes $a \ll 1$ and $a \gg 1$ are reproduced almost exactly, while the maximum error of 0.6% occurs at $a \sim 1$.

Now we need to connect the boundary values $y(0) = y_0$ and $y(1) = 1$ by an interpolating function. This can be done very accurately with the following trick. Let us define an auxiliary function

$$t(x, y) \equiv \left[1 - f_b + \frac{m_b(\bar{x}y)}{m_i(\bar{x})} \right]^{-1}. \quad (\text{A8})$$

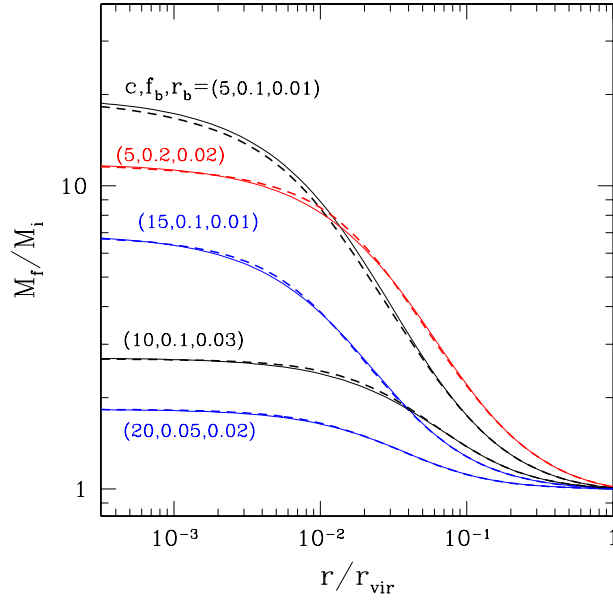


FIG. A6.— Increase of the dark matter mass for the initial NFW models assuming the exponential disk for the final baryon profile. *Solid* lines are the numerical solution, while *dashed* lines are our fitting formulae. Five sets of lines show that our analytical fit (eq. [A11]) reproduces the direct numerical solution for various combinations of the parameters c , f_b , and r_b , with a typical accuracy of better than a few percent.

It satisfies the boundary conditions $t(0, y_0) = y_0$ and $t(1, 1) = 1$. Since $y(x)$ varies slowly near the two bounds, we can use the function $t(x, y)$ to calculate the asymptotic solutions: $y(x \ll 1) \approx t(x, y_0)$ and $y(x \approx 1) \approx t(x, 1)$. The two asymptotes can be linked by a smooth weight function:

$$y(x) = t(x, y_0) e^{-bx} + t(x, 1) (1 - e^{-bx}). \quad (\text{A9})$$

The exponent b that minimizes the error of the fit can be found by an approximate Taylor expansion of eq. (A2) near $x = 0$. We find

$$b = \frac{2y_0}{1 - y_0} \left(\frac{2}{nr_b} - \frac{4c}{3} \right) \left(2.6 + \frac{1 - f_b}{ay_0^{2w}} \right)^{-1}, \quad (\text{A10})$$

where $n = 1$ for the Hernquist model and $n = 3$ for the exponential disk. We have tested the accuracy of eq. (A9) against direct numerical solution for $y(x)$ varying the parameters in the range $4 < c < 20$, $0.02 < f_b < 0.24$, $0.01 < r_b < 0.07$, which should cover most of the cases of interest. We find an average relative error of 2% for the Hernquist model and 1% for the exponential disk. The maximum error is 7% and 4%, respectively, and occurs at $x \sim r_b$.

We can now easily find the final dark matter profile at the contracted radius $x_f = xy(x)$: $M_{\text{dm},f}(xy) = M_{\text{dm},i}(x)$. If desired, the profile can be re-mapped to the grid of initial radii x by interpolation. Let us define the compression function F_M as the ratio of the final dark matter mass to the initial mass at the same radius $xy(x)$:

$$F_M(xy) \equiv \frac{M_{\text{dm},f}(xy)}{M_{\text{dm},i}(xy)} = \frac{M_{\text{dm},i}(x)}{M_{\text{dm},i}(xy)}. \quad (\text{A11})$$

We see that the increase of the dark matter mass due to baryonic infall can be calculated from the initial dark matter profile $M_{\text{dm},i}(x)$ given the transformation $y(x)$. Since we can use an analytic NFW profile, the accuracy of calculating $F_M(x)$ is similar to that for $y(x)$. Figure A6 illustrates that eq. (A11) provides an accurate fitting function at all radii for all values of three independent parameters (c , f_b , r_b).

To summarize, in order to calculate the DM mass profile after contraction analytically one needs to:

- (1) calculate the maximum compression value y_0 using eqs. (A5–A7);
- (2) calculate the exponent b of the weight function using eq. (A10);
- (3) calculate the interpolating function $y(x)$ using eqs. (A8–A9);
- (4) calculate the increase of the enclosed dark matter mass using eq. (A11).

As mentioned above, the mass profiles of the NFW, exponential disk, and Hernquist models are similar at $x \ll r_b, c^{-1}$: $m(x) \propto x^2$. This coincidence leads to a finite enhancement factor for the dark matter mass and density in the central region: $M_{\text{dm},f}(0)/M_{\text{dm},i}(0) = \rho_{\text{dm},f}(0)/\rho_{\text{dm},i}(0) = y_0^{-2}$. Therefore, the central contraction factor y_0 (eq. [A7]) provides a useful measure of the maximum enhancement due to baryonic condensation. The constant contraction factor means that the inner slope of the dark matter distribution after contraction is the same as before contraction. The radius at

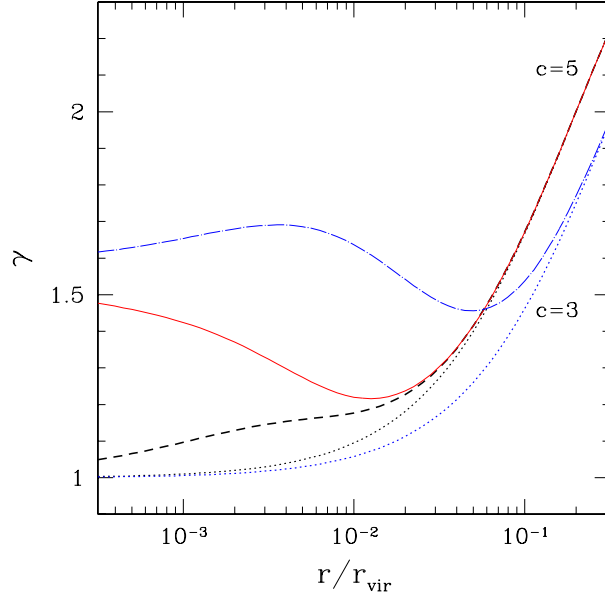


FIG. A7.— The slope of the dark matter profile in cluster MS 2137-23. Dotted lines are the initial NFW profile with $c = 5$ and $c = 3$. Dashed and solid lines are the post-contraction profile for the final baryon distributions given by the Hernquist model and Jaffe model, respectively, with $f_b = 1.3 \times 10^{-3}$ and $r_b = 0.016$. Dot-dashed line shows the post-contraction profile in the case of the Jaffe model with $c = 3$, $f_b = 10^{-2}$ and $r_b = 0.016$.

which this slope is reached, however, depends on the halo concentration and the baryon scale length (see Figure A6). At intermediate radii the post-contraction slope is steeper. In general case, the slope of the final DM profile is different from the initial profile and depends on the shape of the baryon density profile.

Since the value of the inner slope of the dark matter density profile is important for testing CDM models against observations, it is interesting to consider the change of the slope due to the condensation of baryons into a configuration with an arbitrary final density profile. Let the baryon density at $x \ll 1$ be $\rho_b(x) \propto x^{-\nu}$ and therefore the mass $m_b(x) \propto x^{3-\nu}$. If $\nu > 1$, the contraction would not be self-similar with $x_f \propto x$ in the center. Instead, the post-contraction radius would scale as some power of the initial radius: $x_f \propto x^\alpha$. Substituting this into equation (A2) and letting $x \rightarrow 0$, we find $\alpha = (1 + 2w)/(1 + (3 - \nu)w)$. The post-contraction dark mass at the center would scale as $m(x) \propto x^{2/\alpha}$, and therefore the density is

$$\rho(x) \propto x^{-\gamma}, \quad \gamma = \frac{1 + 2w\nu}{1 + 2w}. \quad (\text{A12})$$

For $\nu = 1$, we recover our previous result, $\gamma = 1$, which means that after the contraction of NFW profile by baryons which form an exponential or Hernquist profile, the asymptotic slope at small scales remains the same. For larger ν , the slope γ becomes steeper than the initial slope. Equation (A12) shows (recall that $w \sim 1$) that for $\nu \sim 1 - 2$ the inner slope of the dark matter profile will be quite close to the slope of the baryonic profile.

As an illustration, we consider the profiles with the parameters similar to those of the cluster MS 2137-23 described by Sand et al. (2002, 2004): the virial mass, radius, and concentration are $M_{\text{vir}} \sim 10^{15} M_\odot$ and $r_{\text{vir}} \sim 2$ Mpc, and $c \approx 5$, respectively. At the center of the cluster lies a cD galaxy, which can be well fit by the Jaffe model: $\rho_b \propto x^{-2}(x + r_b)^{-2}$ with $r_b \approx 33$ kpc. Assuming the best fitting mass-to-light ratio $M/L_V = 2.6$ (Sand et al. 2004), the mass of the central galaxy is $1.2 \times 10^{12} M_\odot$. In our notation, the relevant parameters are $f_b = 1.2 \times 10^{-3}$, $r_b = 0.016$.

Figure A7 shows the slope of the post-contraction dark matter density profile appropriate for MS 2137-23 in the range $10^{-3} < x < 10^{-1}$ which is used in the Sand et al. analysis. If the baryon distribution was described by a Hernquist model ($\nu = 1$), the inner slope would tend to $\gamma = 1$, as we discussed above. For the Jaffe model ($\nu = 2$), on the other hand, the slope *steepens* at $x \lesssim 10^{-2}$. According to equation (A12), the asymptotic inner slope is $\gamma \approx 1.6$. This slope is reached faster if we consider a more massive galaxy ($f_b = 10^{-2}$) and a less concentrated cluster ($c = 3$).

REFERENCES

- Arabadjij, J. S., Bautz, M. W., & Garmire, G. P. 2002, *ApJ*, 572, 66
- Balogh, M. L., Pearce, F. R., Bower, R. G., & Kay, S. T. 2001, *MNRAS*, 326, 1228
- Barnes, J. & White, S. D. M. 1984, *MNRAS*, 211, 753
- Bartelmann, M. & Meneghetti, M. 2004, *A&A*, 418, 413
- Binney, J. & Tremaine, S. 1987, *Galactic dynamics* (Princeton: Princeton University Press)
- Blumenthal, G. R., Faber, S. M., Flores, R., & Primack, J. R. 1986, *ApJ*, 301, 27
- Boylan-Kolchin, M. & Ma, C. 2004, *MNRAS*, 349, 1117
- Courteau, S. & Rix, H. 1999, *ApJ*, 513, 561
- Dalal, N. & Keeton, C. R. 2004, *ApJ*, submitted ([astro-ph/0312072](#))
- Dalcanton, J. J., Spergel, D. N., & Summers, F. J. 1997, *ApJ*, 482, 659
- David, L. P., Nulsen, P. E. J., McNamara, B. R., Forman, W., Jones, C., Ponman, T., Robertson, B., & Wise, M. 2001, *ApJ*, 557, 546
- de Blok, W. J. G., Bosma, A., & McGaugh, S. 2003, *MNRAS*, 340, 657
- Dekel, A., Arad, I., Devor, J., & Birnboim, Y. 2003a, *ApJ*, 588, 680
- Dekel, A., Devor, J., & Hetzroni, G. 2003b, *MNRAS*, 341, 326
- Diemand, J., Moore, B., & Stadel, J. 2004, *MNRAS*, submitted, ([astro-ph/0402267](#))
- Dubinski, J. & Carlberg, R. G. 1991, *ApJ*, 378, 496
- Eggen, O. J., Lynden-Bell, D., & Sandage, A. R. 1962, *ApJ*, 136, 748
- El-Zant, A., Hoffman, Y., Primack, J., Combes, F., & Shlosman, I. 2003, *ApJ*, submitted ([astro-ph/0309412](#))
- Ettori, S., Fabian, A. C., Allen, S. W., & Johnstone, R. M. 2002, *MNRAS*, 331, 635
- Flores, R., Primack, J. R., Blumenthal, G. R., & Faber, S. M. 1993, *ApJ*, 412, 443
- Fukushige, T., Kawai, A., & Makino, J. 2004, *ApJ*, submitted ([astro-ph/0306203](#))
- Fukushige, T. & Makino, J. 2001, *ApJ*, 557, 533
- Gao, L., Loeb, A., Peebles, P. J. E., White, S. D. M., & Jenkins, A. 2004, *ApJ*, submitted ([astro-ph/0312499](#))
- Gentile, G., Salucci, P., Klein, U., Vergani, D., & Kalberla, P. 2004, *MNRAS*, in press ([astro-ph/0403154](#))
- Ghigna, S., Moore, B., Governato, F., Lake, G., Quinn, T., & Stadel, J. 1998, *MNRAS*, 300, 146
- Gnedin, O. Y. & Ostriker, J. P. 1999, *ApJ*, 513, 626
- Gnedin, O. Y. & Primack, J. R. 2004, *PRL*, submitted ([astro-ph/0308385](#))
- Gnedin, O. Y. & Zhao, H. 2002, *MNRAS*, 333, 299
- Gonzalez, A. H., Williams, K. A., Bullock, J. S., Kolatt, T. S., & Primack, J. R. 2000, *ApJ*, 528, 145
- Jesseit, R., Naab, T., & Burkert, A. 2002, *ApJ*, 571, L89
- Jimenez, R., Verde, L., & Oh, S. P. 2003, *MNRAS*, 339, 243
- Katayama, H. & Hayashida, K. 2004, *PASJ*, submitted ([astro-ph/0405363](#))
- Kazantzidis, S., Kravtsov, A. V., Zentner, A. R., Allgood, B., Nagai, D., & Moore, B. 2004, *ApJ*, submitted ([astro-ph/0405189](#))
- Klypin, A., Gottlöber, S., Kravtsov, A. V., & Khokhlov, A. M. 1999, *ApJ*, 516, 530
- Klypin, A., Kravtsov, A. V., Bullock, J. S., & Primack, J. R. 2001, *ApJ*, 554, 903
- Klypin, A., Zhao, H., & Somerville, R. S. 2002, *ApJ*, 573, 597
- Kochanek, C. S. & White, M. 2001, *ApJ*, 559, 531
- Koopmans, L. V. E. & Treu, T. 2003, *ApJ*, 583, 606
- Kravtsov, A. V. 1999, PhD thesis, New Mexico State University
- . 2003, *ApJ*, 590, L1
- Kravtsov, A. V., Gnedin, O. Y., & Klypin, A. A. 2004, *ApJ*, in press ([astro-ph/0401088](#))
- Kravtsov, A. V., Klypin, A., & Hoffman, Y. 2002, *ApJ*, 571, 563
- Lewis, G. F., Babul, A., Katz, N., Quinn, T., Hernquist, L., & Weinberg, D. H. 2000, *ApJ*, 536, 623
- Lin, Y., Mohr, J. J., & Stanford, S. A. 2003, *ApJ*, 591, 749
- Loeb, A. & Peebles, P. J. E. 2003, *ApJ*, 589, 29
- Ma, C. & Boylan-Kolchin, M. 2004, *PRL*, submitted ([astro-ph/0403102](#))
- Mamon, G. A. & Lokas, E. L. 2004, *MNRAS*, submitted ([astro-ph/0405466](#))
- Mo, H. J., Mao, S., & White, S. D. M. 1998, *MNRAS*, 295, 319
- Moore, B., Governato, F., Quinn, T., Stadel, J., & Lake, G. 1998, *ApJ*, 499, L5
- Motl, P. M., Burns, J. O., Loken, C., Norman, M. L., & Bryan, G. L. 2004, *ApJ*, 606, 635
- Navarro, J. F., Frenk, C. S., & White, S. D. M. 1997, *ApJ*, 490, 493
- Navarro, J. F., Hayashi, E., Power, C., Jenkins, A. R., Frenk, C. S., White, S. D. M., Springel, V., Stadel, J., & Quinn, T. R. 2004, *MNRAS*, 349, 1039
- Nipoti, C., Treu, T., Ciotti, L., & Stiavelli, M. 2004, *MNRAS*, submitted ([astro-ph/0404127](#))
- Pearce, F. R., Thomas, P. A., Couchman, H. M. P., & Edge, A. C. 2000, *MNRAS*, 317, 1029
- Prada, F., Klypin, A., Flix, J., Martinez, M., & Simonneau, E. 2004, *PRL*, submitted ([astro-ph/0401512](#))
- Reed, D., Governato, F., Verde, L., Gardner, J., Quinn, T., Stadel, J., Merritt, D., & Lake, G. 2004, *MNRAS*, submitted ([astro-ph/0312544](#))
- Rhee, G., Klypin, A., & Valenzuela, O. 2004, *ApJ*, submitted ([astro-ph/0311020](#))
- Ryden, B. S. 1988, *ApJ*, 329, 589
- . 1991, *ApJ*, 370, 15
- Ryden, B. S. & Gunn, J. E. 1987, *ApJ*, 318, 15
- Sand, D. J., Treu, T., & Ellis, R. S. 2002, *ApJ*, 574, L129
- Sand, D. J., Treu, T., Smith, G. P., & Ellis, R. S. 2004, *ApJ*, 604, 88
- Seljak, U. 2002, *MNRAS*, 334, 797
- Simon, J. D., Bolatto, A. D., Leroy, A., & Blitz, L. 2003, *ApJ*, 596, 957
- Swaters, R. A., Madore, B. F., van den Bosch, F. C., & Balcells, M. 2003, *ApJ*, 583, 732
- Tasitsiomi, A., Kravtsov, A. V., Gottlöber, S., & Klypin, A. A. 2004, *ApJ*, 607, 125
- Tissera, P. B. & Dominguez-Tenreiro, R. 1998, *MNRAS*, 297, 177
- Treu, T. & Koopmans, L. V. E. 2002, *ApJ*, 575, 87
- . 2004, *ApJ*, in press ([astro-ph/0401373](#))
- Tyson, J. A., Kochanski, G. P., & dell'Antonio, I. P. 1998, *ApJ*, 498, L107
- Valdarnini, R. 2002, *ApJ*, 567, 741
- van den Bosch, F. C. 2001, *MNRAS*, 327, 1334
- van den Bosch, F. C., Lewis, G. F., Lake, G., & Stadel, J. 1999, *ApJ*, 515, 50
- van den Bosch, F. C. & Swaters, R. A. 2001, *MNRAS*, 325, 1017
- Zeldovich, Y. B., Klypin, A. A., Khlopov, M. Y., & Chechetkin, V. M. 1980, *Soviet J. Nucl. Phys.*, 31, 664